NUMERICAL AND EXPERIMENTAL INVESTIGATION ON NONLINEAR DYNAMIC CHARACTERISTICS OF PLANETARY GEAR TRAIN

Jianwu Zhang, Han Guo

State Key Laboratory of Mechanical System and Vibration, School of Mechanical Engineering, Shanghai Jiao Tong University, China

e-mail: jwuzhang@sjtu.edu.cn; guohan89@gmail.com

Haisheng Yu, Tong Zhang

R&D Center, Corun Hybrid System Technology Co., Ltd., China

e-mail: yhsdg@163.com; zhangtong@chstec.com

A deep hybrid electric vehicle (DHEV) equipped with a Ravigneaux compound planetary gear train (PGT) encounters severe gear whine noises during acceleration in the EV drive mode. For the analysis of vibro-acoustic sources, a 5DOF lumped-parameter vibration model for the PGT dynamic system is established as well as sound pressures radiated from the transmission on a test bench are measured for data processing and recognition. By comparison between numerical and experimental analyses, natural vibration modes of the PGT are examined and high frequency modal resonances in association with the planetary gears are observed only to cause narrow band whine noises. Furthermore, a 2DOF reduced dynamic model for the planetary gears with consideration of nonlinearities such as time-varying mesh stiffness and backlash is proposed, and numerical solutions to bifurcations and dynamic instabilities of the two sets of planetary gears are obtained. It is found that nonlinear vibration behaviour of the long and short planets are major causes of shock and vibration of the hybrid transmission. Severe vibro-acoustic noises excited dominantly by the planetary gears are alleviated after implementing micro-geometry modifications to the PGT.

Keywords: deep hybrid transmission, power-split device, lumped-parameter model, dynamic instability

1. Introduction

Power-split type hybrid systems, which possess synthetic advantages of significant fuel economy, efficient oil-electric power conversion, and external charging free convenience, are potential and important propulsion technologies for low carbon and energy saving vehicles (Zhao *et al.*, 2015). Toyota THS and GM Volt Hybrid are both well-known power-split hybrid systems for mid- and high-class cars (Muta *et al.*, 2004; Meisel, 2011). In these hybrid systems, planetary gear trains (PGTs) are all employed to act as a power-split device (PSD) to realise alternation and utilization of the internal combustion engine (ICE) and electric motor (EM) powers (Zeng and Wang, 2018). Dynamic performance of PGTs, especially operated in heavy loading or at a high speed, is related with eigenmode characteristics, parametric excitations and discontinuities. Nevertheless, modal and parametric resonances and other types of dynamic instabilities of the planetary system may cause mechanical impacts and vibro-acoustic pollutions (Eritenel and Parker, 2009; Lin and Parker, 1999) and even damage to components of the PGTs.

In the earlier analysis of PGT dynamic behaviour, important researches were summarised by Özgüven and Houser (1988). Natural characteristics of the planetary gear train were investigated by Cunliffe *et al.* (1974) using a spring-mass dynamics model. Influence of unequally spaced planets on vibration characteristics of the planetary gear system was studied by Lin and

Parker (2000), applying a more detailed lumped-parameter model counting for two translational and one torsional degrees of freedom. The analysis of more complex natural characteristics of the helical PGT was carried out by Eritenel and Parker (2009), employing a 3D lumped-parameter model of 6DOFs. Torsional vibration characteristics of compound PGTs were analysed by Kahraman (2001), adopting numerical solutions for differential equations governing different types of torsional vibrations.

In dealing with non-modal vibrations of PGTs in heavy loading and at high speeds, nonlinear vibration theories and solution methods are required because the influence of time varying mesh stiffness (TVMS), backlash and transmission error become significant. A survey was made by Wang *et al.* (2003) discussing advances in nonlinear vibration researches published up to 2001. A torsional vibration model for PGTs was established by Farshidianfar and Saghafi (2014), introducing such nonlinear factors as TVMS and backlash, and showing that little variations of system parameters may result in great changes of dynamic behaviour such as periodic and quasi-periodic motions, bifurcations, dynamic instability and chaos. No one shows any interest in dynamic behaviour of two meshed planetary gears.

In the present research, the lumped-parameter dynamic model for the PGT of 5DOFs is established for the analysis of eigenmode properties of the compound PSD of the Ravigneaux type. NVH bench tests for the hybrid transmission are conducted to measure vibration accelerations and sound pressures for not only validation of the numerical modal analysis but also illustration of the nonlinear vibration responses. The nonlinear dynamic model of 2DOFs for high-speed planetary gears in the compound PSD counting for TVMS and backlash is also proposed, and the influence of meshing excitation on dynamic instabilities of the nonlinear system and the related mechanism of vibro-acoustic formation are examined.

2. Dynamic modelling of the compound PGTs

The deep hybrid transmission, in which a Ravigneaux PGT is chosen to be a compound type PSD, has been developed recently for middle-class cars (Zhang *et al.*, 2017b), as shown in Fig. 1, having mainly one ring gear, one planetary carrier, two sun gears, and two sets of equitriangularly spaced planet gears. The small sun gear s_1 meshes three short planet gears b engaged simultaneously with the ring gear r, and the big sun gear s_2 meshes three long planet gears a. On the other side, two groups of planetary gears mesh each other in pairs, and are mounted on the same planetary carrier c. Furthermore, two electric motors, M1 and M2, are connected to s_1 and s_2, respectively, and the ICE is connected to c through a torsional vibration damper (TD). The ring gear r of the compound PSD is engaged to the final reducer, differential, half shafts and the drive wheels. By the compound PSD three input powers are recombined to one output power in the most efficient transmission mode.

For the modal analysis of the compound PGT in torsional vibrations, a lumped-parameter dynamic model is basically presented in Fig. 2. Note that, in each meshing gear pair of the dynamic system, inertia, resilience and damping forces are along the line of action of involute gears. In the torsional vibration system, 10DOFs remain instead of the compound PSD.

As depicted in Fig. 2, define absolute angular displacements of the rotational components θ_c, θ_r, θ_{s_2}, θ_{s_1}, θ_{a_j}, θ_{b_j}. According to the coordinate system, the relative displacements of the components to the carrier can be expressed below

$$\theta_{ic} = \theta_i - \theta_c \tag{2.1}$$

where $i = r, s_2, s_1, a_j$ and b_j and $j = 1, 2, 3$. According to the Lagrangian principle, equilibrium equations of motion governing the mechanical system may be derived in the following form as

$$\frac{d}{dt}\left(\frac{\partial T}{\partial \dot{q}_k}\right) - \frac{\partial T}{\partial q_k} + \frac{\partial R}{\partial \dot{q}_k} + \frac{\partial V}{\partial q_k} = Q_k \tag{2.2}$$
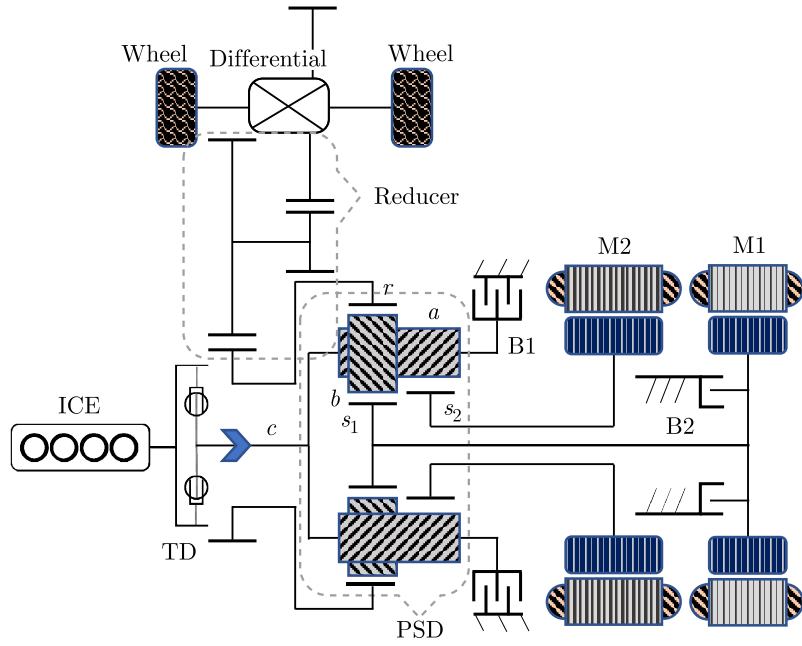
Fig. 1. Configuration of the hybrid powertrain with a compound PSD

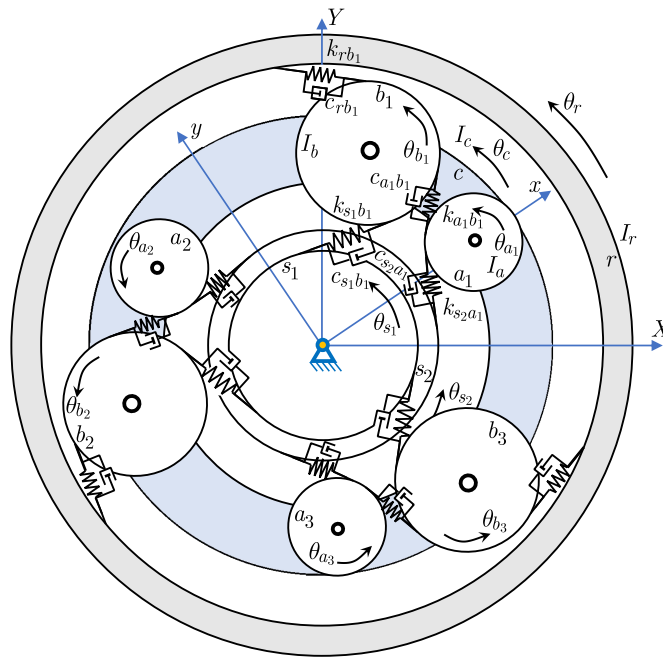

Fig. 2. The lumped-parameter dynamic model of the compound PSD

where T, V, and R are functions corresponding to kinetic, potential and dissipated energies of the systems, Q_k is the k-th term of generalized forces vector, and the k-th order vector $\mathbf{q}_{pt}$ of the generalized coordinates given below

$$\mathbf{q}_{pt} = [\theta_c, \theta_r, \theta_{s_2}, \theta_{s_1}, \theta_{a_1 c}, \theta_{b_1 c}, \ldots, \theta_{a_3 c}, \theta_{b_3 c}]^{\mathrm{T}} \tag{2.3}$$

For details, the kinetic, potential and dissipated energy functions, T, V and R, can be presented in the following form as

$$T = \frac{1}{2}I_c\dot{\theta}_c^2 + \frac{1}{2}\sum_{j=1}^{N}m_{a0}(\dot{\theta}_c r_{ac})^2 + \frac{1}{2}\sum_{j=1}^{N}m_{b0}(\dot{\theta}_c r_{bc})^2 + \frac{1}{2}I_r\dot{\theta}_r^2 + \frac{1}{2}I_{s_2}\dot{\theta}_{s_2}^2 + \frac{1}{2}I_{s_1}\dot{\theta}_{s_1}^2$$

$$+ \frac{1}{2}\sum_{j=1}^{N}I_a(\dot{\theta}_c + \dot{\theta}_{a_j}c)^2 + \frac{1}{2}\sum_{j=1}^{N}I_b(\dot{\theta}_c + \dot{\theta}_{b_jc})^2$$

$$V = \frac{1}{2}\sum_{j=1}^{N}k_{s2a}[r_a\theta_{a_jc} + r_{s_2}(\theta_{s_2} - \theta_c)]^2 + \frac{1}{2}\sum_{j=1}^{N}k_{s_1b}[r_b\theta_{b_jc} + r_{s_1}(\theta_{s_1} - \theta_c)]^2$$

$$+ \frac{1}{2}\sum_{j=1}^{N}k_{ab}(r_a\theta_{a_jc} + r_b\theta_{b_jc})^2 + \frac{1}{2}\sum_{j=1}^{N}k_{rb}[r_r(\theta_r - \theta_c) - r_b\theta_{b_jc}]^2 \qquad (2.4)$$

$$R = \frac{1}{2}\sum_{j=1}^{N}c_{s2a}[r_a\dot{\theta}_{a_jc} + r_{s_2}(\dot{\theta}_{s_2} - \dot{\theta}_c)]^2 + \frac{1}{2}\sum_{j=1}^{N}c_{s_1b}[r_b\dot{\theta}_{b_jc} + r_{s_1}(\dot{\theta}_{s_1} - \dot{\theta}_c)]^2$$

$$+ \frac{1}{2}\sum_{j=1}^{N}c_{ab}(r_a\dot{\theta}_{a_jc} + r_b\dot{\theta}_{b_jc})^2 + \frac{1}{2}\sum_{j=1}^{N}c_{rb}[(r_r(\dot{\theta}_r - \dot{\theta}_c) - r_b\dot{\theta}_{b_jc}]^2$$

where m_{a0}, m_{b0} and r_{ac}, r_{bc} represent masses and radii of the planetary gears a, b, respectively, the number of planetary gears $N = 3$, $j = 1, 2, 3$ represents order number of the planetary gear, and k_{rb}, k_{s_2a}, k_{s_1b} and k_{ab} are four types of gear meshing stiffnesses, c_{rb}, c_{s_2a}, c_{s_1b} and c_{ab} are damping factors of the four types of gear pairs.

Torques of the traction components, M1, M2, and ICE, are applied to s_1, s_2 and c during working modes of the hybrid system, respectively. Meanwhile r bears resistant torques from the vehicle drive wheels and driveline. The vector of generalized forces can be expressed as follows

$$\mathbf{Q}_{pt} = [T_c, T_r, T_{s_2}, T_{s_1}, 0, 0, 0, 0, 0, 0]^{\mathrm{T}} \qquad (2.5)$$

Substitution of Eqs. (2.3)-(2.5) into Eq. (2.2) results in equilibrium equations of motion of the dynamic system in simultaneous form as follows

$$I_c\ddot{\theta}_c + N(I_a + I_b + r_{ac}^2 m_{a0} + r_{bc}^2 m_{b0})\ddot{\theta}_c + \sum_{j=1}^{N}I_a\ddot{\theta}_{a_jc} + \sum_{j=1}^{N}I_b\ddot{\theta}_{b_jc}$$

$$+ \sum_{j=1}^{N}c_{s2a}(r_{s_2}^2\dot{\theta}_c - r_{s_2}^2\dot{\theta}_{s_2} - r_a r_{s_2}\dot{\theta}_{a_jc}) + \sum_{j=1}^{N}c_{s_1b}(r_{s_1}^2\dot{\theta}_c - r_{s_1}^2\dot{\theta}_{s_1} - r_b r_{s_1}\dot{\theta}_{b_jc})$$

$$+ \sum_{j=1}^{N}c_{rb}(r_r^2\dot{\theta}_c - r_r^2\dot{\theta}_r + r_r r_b\dot{\theta}_{b_jc}) + \sum_{j=1}^{N}k_{s2a}(r_{s_2}^2\theta_c - r_{s_2}^2\theta_{s_2} - r_a r_{s_2}\theta_{a_jc})$$

$$+ \sum_{j=1}^{N}k_{s_1b}(r_{s_1}^2\theta_c - r_{s_1}^2\theta_{s_1} - r_b r_{s_1}\theta_{b_jc}) + \sum_{j=1}^{N}k_{rb}(r_r^2\theta_c - r_r^2\theta_r + r_r r_b\theta_{b_jc}) = T_c$$

$$I_r\ddot{\theta}_r + \sum_{j=1}^{N}c_{rb}(r_r^2\dot{\theta}_r - r_r^2\dot{\theta}_c - r_r r_b\dot{\theta}_{b_jc}) + \sum_{j=1}^{N}k_{rb}(r_r^2\theta_r - r_r^2\theta_c - r_r r_b\theta_{b_jc}) = T_r \qquad (2.6)$$

$$I_{s_2}\ddot{\theta}_{s_2} + \sum_{j=1}^{N}c_{s2a}(r_{s_2}^2\dot{\theta}_{s_2} - r_{s_2}^2\dot{\theta}_c + r_{s_2} r_a\dot{\theta}_{a_jc}) + \sum_{j=1}^{N}k_{s2a}(r_{s_2}^2\theta_{s_2} - r_{s_2}^2\theta_c + r_{s_2} r_a\theta_{a_jc}) = T_{s_2}$$

$$I_{s_1}\ddot{\theta}_{s_1} + \sum_{j=1}^{N}c_{s_1b}(r_{s_1}^2\dot{\theta}_{s_1} - r_{s_1}^2\dot{\theta}_c + r_{s_1} r_b\dot{\theta}_{b_jc}) + \sum_{j=1}^{N}k_{s_1b}(r_{s_1}^2\theta_{s_1} - r_{s_1}^2\theta_c + r_{s_1} r_b\theta_{b_jc}) = T_{s_1}$$

$$I_a\ddot{\theta}_{a_jc} + I_a\ddot{\theta}_c + c_{s2a}(r_{s_2} r_a\dot{\theta}_{s_2} - r_{s_2} r_a\dot{\theta}_c + r_a^2\dot{\theta}_{a_jc}) + c_{ab}(r_a^2\dot{\theta}_{a_jc} + r_a r_b\dot{\theta}_{b_jc})$$

$$+ k_{ab}(r_a^2\theta_{a_jc} + r_a r_b\theta_{b_jc}) + k_{s2a}(r_{s_2} r_a\theta_{s_2} - r_{s_2} r_a\theta_c + r_a^2\theta_{a_jc}) = 0$$

$$I_b\ddot{\theta}_{b_jc} + I_b\theta_c + c_{s_1b}(r_{s_1}r_b\dot{\theta}_{s_1} - r_{s_1}r_b\dot{\theta}_c + r_b^2\dot{\theta}_{b_jc}) + c_{ab}(r_ar_b\dot{\theta}_{a_jc} + r_b^2\dot{\theta}_{b_jc})$$
$$+ c_{rb}(r_rr_b\dot{\theta}_c - r_rr_b\dot{\theta}_r + r_b^2\dot{\theta}_{b_jc}) + k_{s_1b}(r_{s_1}r_b\theta_{s_1} - r_{s_1}r_b\theta_c + r_b^2\theta_{b_jc})$$
$$+ k_{ab}(r_ar_b\theta_{a_jc} + r_b^2\theta_{b_jc}) + k_{rb}(r_rr_b\theta_c - r_rr_b\theta_r + r_b^2\theta_{b_jc}) = 0$$

The mathematical model in Eqs. (2.6) may be presented in the following matrix form as

$$\mathbf{M}_{pt}\ddot{\mathbf{q}}_{pt} + \mathbf{C}_{pt}\dot{\mathbf{q}}_{pt} + \mathbf{K}_{pt}\mathbf{q}_{pt} = \mathbf{Q}_{pt} \tag{2.7}$$

where $\mathbf{M}_{pt}$, $\mathbf{K}_{pt}$ and $\mathbf{C}_{pt}$ are mass, stiffness and damping matrices, respectively. Inertia parameters of each component are listed in Table 1, and gear base circle radii and planet center distances are given in Table 2.

Table 1. Mass and moments of inertia of the compound PGT components

Equivalent parameter symbol	Value	Equivalent parameter symbol	Value
Planetary carrier I_c'	$0.00363\,\text{kg m}^2$	Long planet I_a	$2.17 \cdot 10^{-5}\,\text{kg m}^2$
ICE crank-rod mechanism I_e	$0.14\,\text{kg m}^2$	Short planet I_b	$3.55 \cdot 10^{-5}\,\text{kg m}^2$
Ring gear I_r	$8.97\,\text{kg m}^2$	Long planet m_{a0}	$0.129\,\text{kg}$
M1 and sun gear 1 I_{s_1}	$0.0486\,\text{kg m}^2$	Short planet m_{b0}	$0.151\,\text{kg}$
M2 and sun gear 2 I_{s_2}	$0.0805\,\text{kg m}^2$		

Table 2. Base circle radii and center distances [m]

Base circle radius	Value	Centre distance	Value
Ring gear r_r	0.565	Long planet and sun gear 2 r_{ac}	0.0397
Sun gear 1 r_{s_1}	0.0178	Short planet and sun gear 1 r_{bc}	0.0415
Sun gear 2 r_{s_2}	0.0241		
Long planet gear r_a	0.0146		
Short planet gear r_b	0.0197		

The integral potential energy method is widely applied theoretically for determining spur and helical gear mesh stiffnesses (Gu *et al.*, 2015; Wang *et al.*, 2018). Gear teeth in mesh are assumed to be cantilever beams. Accordingly, the total potential energy of a gear tooth under loading is composed of Hertzian contact energy U_h, bending deformation energy U_b, shear deformation energy U_s, axial stain energy U_a and gear flank deformation energy U_f. It can be expressed in the following form as (Zhang *et al.*, 2017b)

$$U_h = \frac{F^2}{2k_h} \qquad U_b = \frac{F^2}{2k_b} \qquad U_s = \frac{F^2}{2k_s} \qquad U_a = \frac{F^2}{2k_a} \qquad U_f = \frac{F^2}{2k_f} \tag{2.8}$$

where F is the normal force applied on the tooth, k_h, k_b, k_s, k_a and k_f are, respectively, Hertz contact stiffness, bending stiffness, shear stiffness, axial compression stiffness and gear flank stiffness of the cantilever beam, detailed formulations of which may be found (Zhang *et al.*, 2017b).

During loading of the gear pair in rotation, the mesh stiffness of the meshing gears varies periodically and is a time-varying function from meshing-in to meshing-out of the gear teeth. For convenience in an engineering application, the TVMS may be expanded to be a Fourier series (Zhang *et al.*, 2017b)

$$\widetilde{k}_{ij}(t) = \overline{k}_{ij} + \sum_{l=1}^{K_l} \cos(l\omega_m t + \varphi_l) \tag{2.9}$$

where $\widetilde{k}_{ij}(t)$ and $\overline{k}_{ij}$ represent a periodical function and the mean value of TVMS of the gear pair i and j. K_l and φ_l are the stiffness amplitude and initial phase of the l-th harmonic component, ω_m is the radial meshing frequency of the mating gears. In the present research, TVMS is represented by taking the first 6 terms of the Fourier series as an approximation, whose accuracy can be verified sufficiently high enough by estimating the rest terms of the Fourier series in proportion to the real mesh stiffness in a much lower order of magnitude (Hedlund and Lehtovaara, 2008). Accordingly, the TVMSs of the four types of gear pairs in the compound PGT are obtained but not presented herein for limitation of paper length (Zhang $et\ al.$, 2017a).

In the linear modal analysis for the dynamic system of the compound PGT, only average mesh stiffnesses of each gear pair are considered, unless nonlinear vibration responses become significant.

3. Natural frequency analysis

Assuming ω_0 and ω_d are undamped and damped eigenfrequencies of the gear vibration system, and there exists a formula such that $\omega_d = \omega_0\sqrt{1-\zeta^2}$, where ζ is the damping ratio of the tooth mesh which commonly lies between 0.03 and 0.17 (Kasuba and Evans, 1981). When ζ is equal to 0.17, $\omega_d \approx 0.985\omega_0$, thus, the damping ratio has little influence on eigenfrequencies of the gear vibration system.

By ignoring damping effects, the math model in Eq. (2.7) is reduced to the free vibration equations of the PGT in the following form as

$$\mathbf{M}_{pt}\ddot{\mathbf{q}}_{pt} + \mathbf{K}_{pt}\mathbf{q}_{pt} = \mathbf{0} \tag{3.1}$$

Further, the corresponding eigenequations may be reconstructed of the following form as

$$(\mathbf{K}_{pt} - \omega_i^2\mathbf{M}_{pt})\mathbf{q}_{pt} = \mathbf{0} \tag{3.2}$$

Since $\mathbf{q}_{pt} \neq \mathbf{0}$, the determinant in Eq. (3.2) must be equal to zero. The eigenvalues of the determinant can be determined by Liouville's theorem. For each of the natural frequencies, iterations of the generalized coordinates in Eq. (3.2) lead to the corresponding eigenvectors representing modal shapes of the dynamic system.

Table 3. Eigenfrequencies and modes of the compound PGT in EV drive mode

Order	Frequency [Hz]	Mode (component)
1	5.60	Ring
2	42.89	Sun 1
3	56.90	Sun 2
4, 5, 6	2365.23	Long planet
7, 8, 9	3381.58	Short planet

In the electric drive mode, the carrier c is clamped down by the brake B1. The solutions to eigenfrequencies and modes for torsional vibrations of the PGT can be obtained by using Eq. (3.2) and presented in Table 3. On a sharp contrast, eigenfrequencies of the three central components are all lower than 100 Hz, but those corresponding to the long and short planetary gears are much higher in comparison.

4. NVH bench test and analysis

For the purpose of identifying the whine noise sources radiated from the hybrid transmission while the EV is accelerated in the electric drive mode from standstill, an NVH test bench is established in a semi-silence room, as shown in Fig. 3.
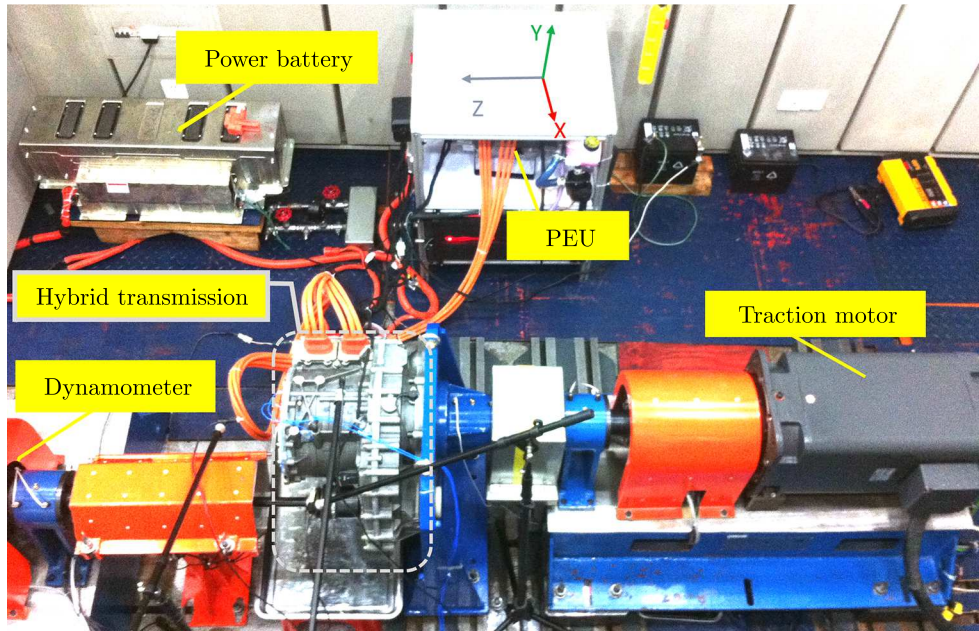
Fig. 3. NVH test bench for the hybrid transmission

In addition to the hybrid transmission, the test bench mainly consists of a traction motor, dynamometer, group of test sensors, and a data acquisition system. These sensors are, respectively, three accelerometers fixed on the housing surface and three microphones placed close to the corresponding accelerometers around the transmission.

In the simulation of pure electric drive mode condition for the NVH test, for example, the carrier c is clamped down by B1, and the motor M2 speeds up and drives through the PSD in the hybrid transmission the dynamometer (inertia effect of the vehicle) from 50 to 700 rpm, being equivalent to the real vehicle launches from the standstill to a medium speed. Experimental data acquired by the sensors are recorded and treated by a post-process system of the LMS Test.Lab software. Test results of dynamic responses for acceleration and vibro-acoustic pressure in frequency domains are plotted with an input speed increase of s_2 (M2) in Figs. 4a and 4b. As observed from the waterfall plots in Fig. 4, the two eigenfrequencies of the long and short planetary gears are easily recognized in rectangular windows.

Many slants appear in the plots in Fig. 4a and mean that the meshing frequencies of the planets rise proportionally with an increase of the electric motor speed. During the run-up process, except for the two planet modal resonances, as observed in Fig. 4b, high levels of sound pressures imply that severe self-excited and parametric resonances occur between the two planet eigenfrequencies, especially in the neighbourhood of the eigenfrequency of the planet b.

5. Nonlinear vibrations of the PGT

5.1. The dynamic system modelling

According to the above modal analysis, the central components r, s_1 and s_2 are fixed to the ground from a viewpoint of relative motion, since eigenfrequencies of the central parts are much lower in comparison with those of the planets. In the electric drive mode, the carrier c is held still by the brake B1. By a similar modal analysis of the dynamic system with fixed central parts, it is easily found that natural frequencies of the three sets of planetary gears are kept almost unchanged. In this occasion, the complete PGT may be replaced with the reduced system of the planets, ignoring modal effects of the central parts. In the other hand, due to equilateral
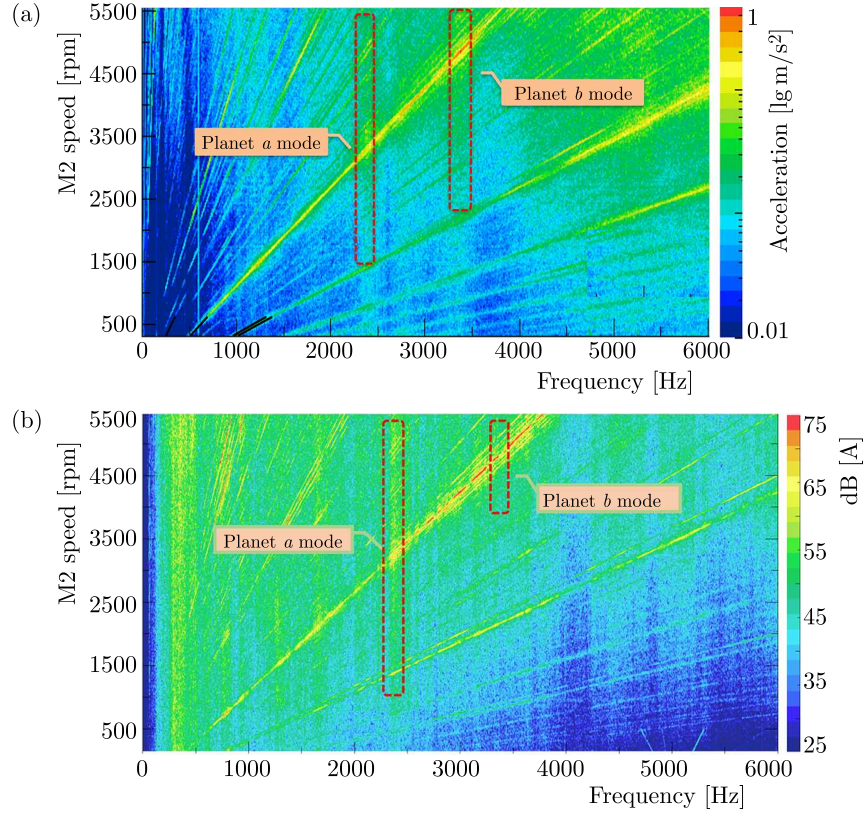
Fig. 4. Waterfall plots of dynamic responses for the compound PSD: (a) vibration accelerations on the housing surface, (b) vibro-acoustic pressures near the housing

triangle arrangement of the three pairs of planets on the rigid carrier, the reduced system can be further simplified by the axial symmetry of rotation to the one third system of one pair of planets for nonlinear vibration analysis. As a result, set $\theta_r = 0$, $\theta_{s_1} = \theta_{s_2} = 0$ and $\theta_c = 0$, in Fig. 2, the simplified dynamic model of two degrees of freedom for the long and short planetary gears is further developed, in which nonlinear factors such as TVMS, backlash and damping of the gear pairs are taken into consideration.

Driving torques of M2 and M1 are applied simultaneously to the long and short planetary gears, without deviations due to manufacturing and assembly.

The equilibrium equations of motion for the planet system can be presented in the following form

$$
\begin{aligned}
&I_a \ddot{\theta}_a + c_{s_2a} r_a^2 \dot{\theta}_a + c_{ab} r_a (r_a \dot{\theta}_a + r_b \dot{\theta}_b) + \widetilde{k}_{s_2a} r_a f(r_a \theta_a) + \widetilde{k}_{ab} r_a f(r_a \theta_a + r_b \theta_b) = T_a \\
&I_b \ddot{\theta}_b + c_{rb} r_b^2 \dot{\theta}_b + c_{s_1b} r_b^2 \dot{\theta}_b + c_{ab} r_b (r_a \dot{\theta}_a + r_b \dot{\theta}_b) + \widetilde{k}_{rb} r_b f(r_b \theta_b) + \widetilde{k}_{s_1b} r_b f(r_b \theta_b) \\
&\quad + \widetilde{k}_{ab} r_b f(r_a \theta_a + r_b \theta_b) = T_b
\end{aligned}
\tag{5.1}
$$

where r_a and r_b are base circle radii of long and short planet gears, c_{ij} are damping coefficients, $\widetilde{k}_{ij}$ are time-varying mesh stiffnesses of meshing gears i and j, and $f(u)$ is the displacement function describing gear backlash, $T_a = T_{s_2} r_{s_2}/(3r_a)$ and $T_b = T_{s_1} r_{s_1}/(3r_b)$. For the sake of intuition, the following coordinate transformations are introduced

$$
u_a = r_a \theta_a \qquad u_b = r_b \theta_b
\tag{5.2}
$$

Substitution of Eqs. (5.2) into Eq. (5.1) result in vibration equations of the system in terms of displacement along the line of action

$$\frac{I_a}{r_a^2}\ddot{u}_a + c_{s_2a}\dot{u}_a + c_{ab}(\dot{u}_a + \dot{u}_b) + \widetilde{k}_{s_2a}f(u_a) + \widetilde{k}_{ab}f(u_a + u_b) = \frac{T_a}{r_a}$$

$$\frac{I_b}{r_b^2}\ddot{u}_b + c_{rb}\dot{u}_b + c_{s_1b}\dot{u}_b + c_{ab}(\dot{u}_a + \dot{u}_b) + \widetilde{k}_{rb}f(u_b) + \widetilde{k}_{s_1b}f(u_b) + \widetilde{k}_{ab}f(u_a + u_b) = \frac{T_b}{r_b}$$

(5.3)

And the damping coefficients of the gear pairs can be calculated below

$$c_{ij} = 2\zeta\sqrt{\frac{\overline{k}_{ij}}{r_i^2/I_i + r_i^2/I_j}}$$

(5.4)

where ζ is the damping ratio in a range of 0.03-0.17 and taken to 0.10, herein, r_i, r_j and I_i, I_j are base circle radii and moments of inertia of meshing gears.

The displacement function for backlashes of meshing gear teeth introduced into Eq. (5.1) can be expressed in the following piecewise form

$$f(u) = \begin{cases} u - b_l & \text{for} & u > b_l \\ 0 & \text{for} & -b_l \leqslant u \leqslant b_l \\ 3pt]u + b & \text{for} & u < -b_l \end{cases}$$

(5.5)

where $b_l = b_n \cos\beta/2$ and b_n is the normal backlash. Backlashes of the four gear pairs are all equal to 0.12 mm, and the helical angle β takes 23 deg.

5.2. Nondimensionalization of the math modelling

By introducing basic parameters $x(\tau) = u(t)/b_l$, $\omega_n = \sqrt{\overline{k}_{ab}/(r_a^2 I_a + r_b^2 I_b)}$, $\widehat{m}_a = \omega_n^2 I_a/r_a^2$, $\widehat{m}_b = \omega_n^2 I_b/r_b^2$, $F_a = T_a/(r_a b_l)$, $F_b = T_b/(r_b b_l)$, $\tau = t\omega_n$, the geverning equations of the vibration system in Eqs. (5.3) and (5.5) may be transformed and rewritten down in a dimensionless form

$$\widehat{m}_a\ddot{x}_a + \widehat{c}_{s_2a}\dot{x}_a + \widehat{c}_{ab}(\dot{x}_a + \dot{x}_b) + \widetilde{k}_{s_2a}\widehat{f}(x_a) + \widetilde{k}_{ab}\widehat{f}(x_a + x_b) = F_a$$

$$\widehat{m}_b\ddot{x}_b + \widehat{c}_{rb}\dot{x}_b + \widehat{c}_{s_1b}\dot{x}_b + c_{ab}(\dot{x}_a + \dot{x}_b) + \widetilde{k}_{rb}\widehat{f}(x_b) + \widetilde{k}_{s_1b}\widehat{f}(x_b) + \widetilde{k}_{ab}\widehat{f}(x_a + x_b) = F_b$$

(5.6)

and

$$\widehat{f}(x) = \begin{cases} x - 1 & \text{for} & x > 1 \\ 0 & \text{for} & -1 \leqslant x \leqslant 1 \\ x + 1 & \text{for} & x < -1 \end{cases}$$

(5.7)

where $\widehat{c}_{ij}$ are equivalent damping coefficients of the gear pairs i and j. In Eq. (5.1), $f(u)$ is a discontinuous function describing the gear pair backlash in the angular displacement. It is also referred to Eq. (5.5) in the linear displacement and Eq. (5.7) in a dimensionless form. Consequently, the dynamic model of the planetary gears equivalent to the original torsional vibration model is presented in Fig. 5.

For the analysis of nonlinear behaviour of the dynamic system, the vector of state variables **x** is further introduced of the following form

$$\mathbf{x} = [x_1, x_2, x_3, x_4]^{\mathrm{T}}$$

(5.8)

Then, the differential equations in Eq. (5.6) may be transformed into a set of state equations below

$$\dot{x}_1 = x_3 \qquad \dot{x}_2 = x_4$$

$$\dot{x}_3 = \frac{F_a}{\widehat{m}_a} + \frac{1}{\widehat{m}_a}[-\widehat{c}_{s_2a}x_3 - \widehat{c}_{ab}(x_3 + x_4) - \widetilde{k}_{s_2a}\widehat{f}(x_1) - \widetilde{k}_{ab}\widehat{f}(x_1 + x_2)]$$

$$\dot{x}_4 = \frac{F_b}{\widehat{m}_b} + \frac{1}{\widehat{m}_b}[-\widehat{c}_{rb}x_4 - \widehat{c}_{s_1b}x_4 - \widehat{c}_{ab}(x_3 + x_3) - \widetilde{k}_{rb}\widehat{f}(x_2) - \widetilde{k}_{s_1b}\widehat{f}(x_2) - \widetilde{k}_{ab}\widehat{f}(x_1 + x_2)]$$
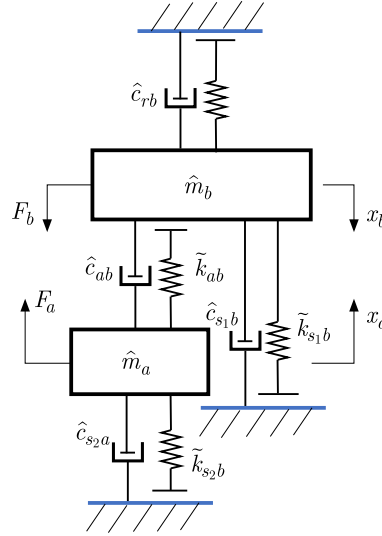
(5.9)

Fig. 5. The equivalent vibration model

The equilibrium equations of motion in Eq. (5.6) are transformed to the set of state equations in Eq. (5.9) by introduction of the vector of state variables $\mathbf{x} = [x_1, x_2, x_3, x_4]^{\mathrm{T}} = [x_a, x_b, \dot{x}_a, \dot{x}_b]^{\mathrm{T}} = [x_1, x_2, \dot{x}_1, \dot{x}_2]^{\mathrm{T}}$. Initial conditions of the dynamic system for the vector of state variables $\mathbf{x}(0)$ are dependent on average displacements and zero velocities in the steady state.

5.3.   Solution and analysis

The numerical solution to nonlinear state equations Eq. (5.9) is performed by an implicit fourth-order Runge-Kutta method and MATLAB. Phase trajectories of the planetary gears are obtained with consideration of different parametric excitations like time varying mesh stiffness and teeth backlash.

Whenever the rotational speed ω of the traction motor M2 is increased to 3750 rpm, equivalently, the dynamic system is operated at the dimensionless mesh frequency $\Omega = 3.46$ ($\Omega = \omega_{\mathrm{m}}/\omega_n$), numerical results of phase trajectories for the planets a and b are plotted in Figs. 6a and 6b. As observed, dynamic behaviours of the long and short planetary gears appear periodic in limit circles, and the peak-to-peak vibration amplitude values are about 4.
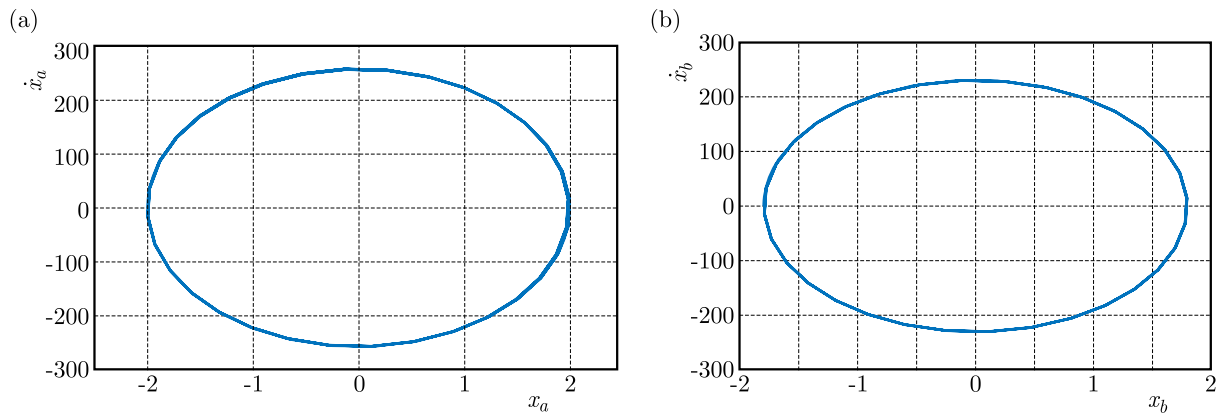

Fig. 6. Phase trajectories of the dynamic system operated at $\Omega = 3.46$: (a) planet a, (b) planet b

Test results of frequency responses for housing accelerations and sound pressures are acquired from the NVH bench test and are given in Figs. 7a and 7b. As observed, peaks of housing

accelerations and sound pressures take place at $\Omega = 3.46$ and $2\Omega = 6.92$ corresponding to the mesh frequency and its doubling, and maximum amplitudes for acceleration and sound pressure are measured to be about $2.9\,\mathrm{m/s^2}$ and $72.1\,\mathrm{dB}$.
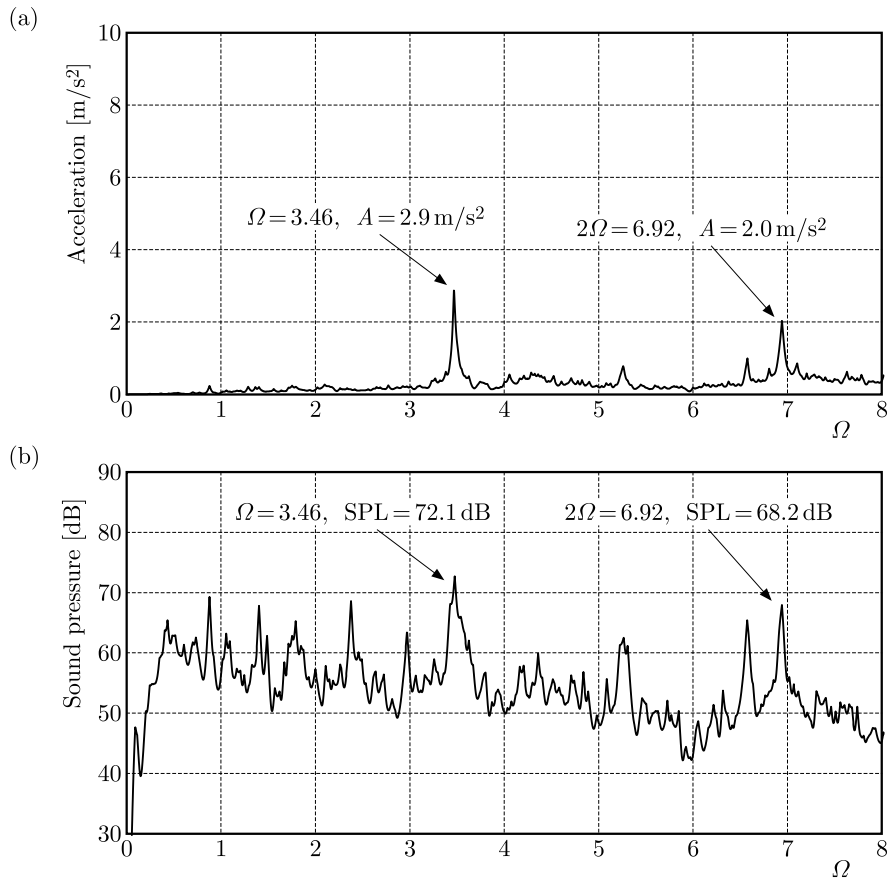
(a)

(b)

Fig. 7. Test results of frequency responses for the dynamic system operated at $\Omega = 3.46$:
(a) acceleration on the housing surface, (b) sound pressure near the housing

Whenever the speed of M2 continues to rise up to about $4300\,\mathrm{rpm}$, equivalently, the dynamic system is operated at $\Omega = 3.97$, the phase trajectories of the dynamic system are presented in Figs. 8a and 8b. As observed, motions of the long and short planets are still periodic but pseudo harmonic. In comparison, however, with an increase of the power input to the system, vibration amplitudes in velocity for the present system become about 2 times of those for the previous one. Motions of the 2-planet system bifurcate and appear unstable between 2 stable limit circles.

Test results of frequency responses for housing acceleration and sound pressure are obtained to be similar to Fig. 7, but the peaks of housing acceleration and sound pressure also appear to be $4.6\,\mathrm{m/s^2}$ and $74.5\,\mathrm{dB}$ at $\Omega = 3.97$, being 58% higher than those of the previous one.

Whenever the speed of M2 rises up to $4700\,\mathrm{rpm}$, equivalently, the dynamic system is operated at $\Omega = 4.34$, numerical solutions to phase trajectories of the long and short planets are plotted in Figs. 9a and 9b. As observed, the vibration behaviour also looks periodic and both similar in pattern, and maximum amplitudes in velocity for the present case become 2 times of those for the previous case again. It is interesting that bifurcations of motions of both the planets a and b appear again, and the nonlinear behaviour seems to be unaffected by each other. In comparison, the unstable annular area of the previous case in Figs. 8a and 8b are further separated into two unstable annular areas in mutual attraction of the present one in Figs. 9a and 9b.
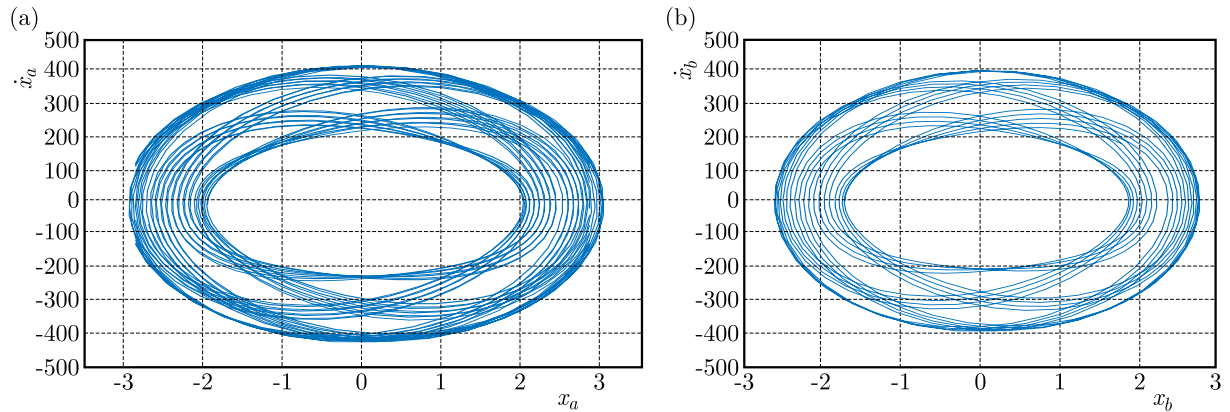
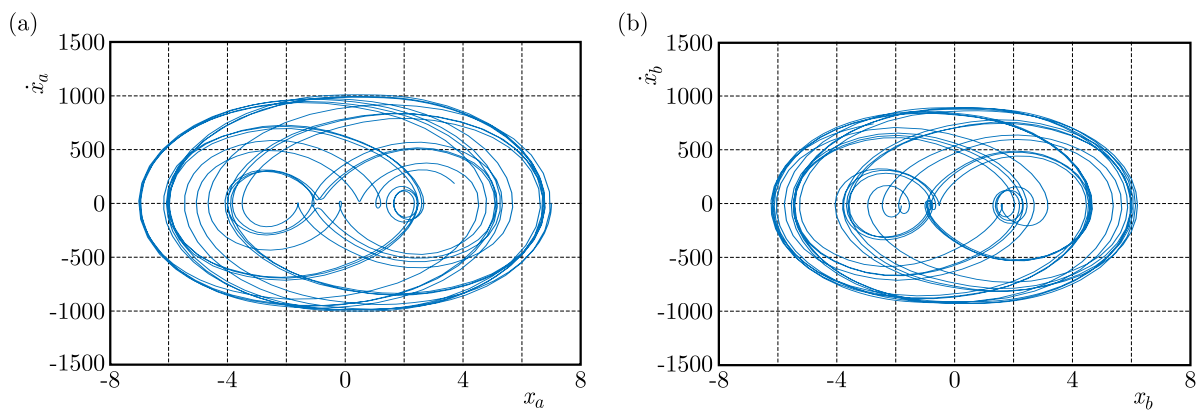Fig. 8. Phase trajectories of the dynamic system operated at $\Omega = 3.97$: (a) planet a, (b) planet b

Fig. 9. Phase trajectories of the dynamic system operated at $\Omega = 4.34$: (a) planet a, (b) planet b

Test results obtained from the experiments for the frequency responses of housing acceleration and sound pressure are obtained to be also similar to those in Fig. 7, but the peaks of housing acceleration and sound pressure also appears to be about $8.8\,\mathrm{m/s^2}$ and $80.8\,\mathrm{dB}$ at the mesh frequency $\Omega = 4.34$, being much higher than those at $\Omega = 3.46$.

The above numerical examples and experiments show that whine noise intensities upgrade to a very high level with step-by-step increases of M2 operation speed. It is obviously recognized that the most of vibro-acoustic energy is generated due to self-excited and parametric resonances of the planetary gears, as clearly shown in Fig. 4 by the line of time-frequency responses, starting from the eigenfrequencies, 2365 and 3382 Hz, of the planet a and the planet b.

The present research shows that dynamic instabilities of the planetary gears in heavy loading and at high speeds are the major cause of parametric resonances leading to broad band shock and vibration. For improving NVH performance of the compound PGT, micro-geometry modifications are made to central and planetary gears to mesh each other in a greater contact area by a contact imprinting test of the meshing gears in the transmission assembly (Guo *et al.*, 2018). Afterwards, NVH measurements are also made in the test bench under the same EV drive conditions. Both frequency responses for sound pressures of the PGT before and after modifications are given in Fig. 10, see the peak level reduced from 86.5 dB to 81.0 dB. The waterfall plot for acoustic pressures of the PGT after modifications is presented in Fig. 11. As observed, the whine noise induced due to dynamic instability of the planetary gears is obviously decreased in comparison with that in Fig. 4b.
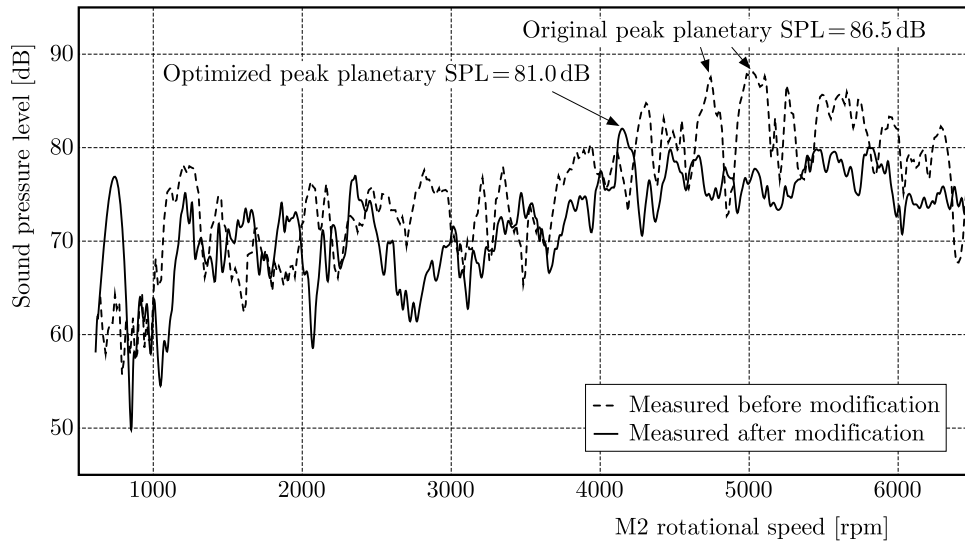
Fig. 10. Comparison of test results for sound pressures after and before modifications
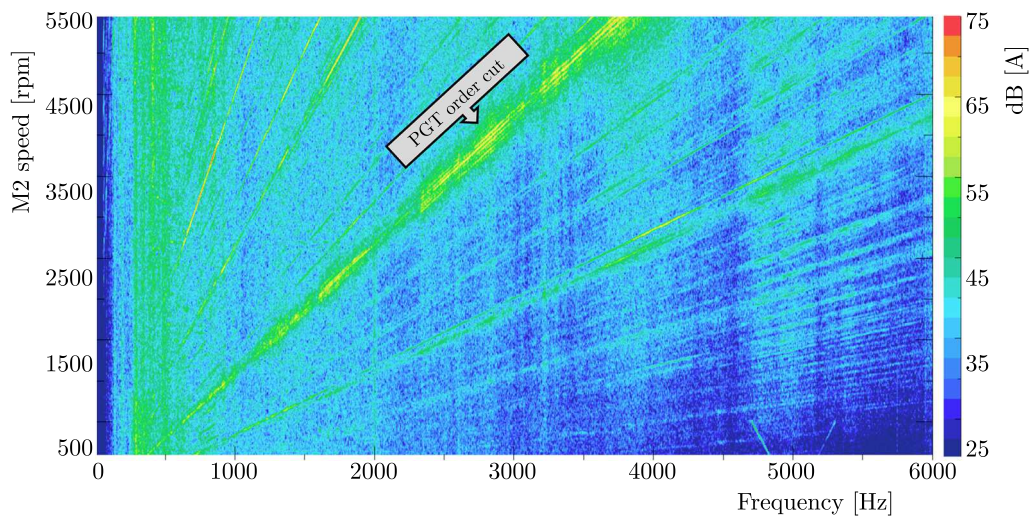

Fig. 11. Waterfall plot for vibro-acoustic pressures of the hybrid transmission after modifications

6. Conclusion

For the investigation to vibro-acoustic sources of severe whine noise radiated from the deep hybrid transmission, numerical analyses and bench tests are carried out. The simultaneous equilibrium equations of motion for the reduced 5DOFs lumped-parameter vibration system of the compound PGT are developed, based upon the Lagrange principle. On the other hand, vibrations and acoustic radiations of the transmission are measured and evaluated on the test bench in a variety of electric drive conditions. Numerical solutions for eigenmode properties of the PGT are produced and found in fairly good agreement with those obtained from the bench tests.

After ordinary modal analysis of the dynamic system of 5 degrees of freedom, the emphasis is also placed on the mechanism of vibro-acoustic formation in the hybrid transmission. For nonlinear investigation on dynamic instabilities of the PGT, the dynamic system is further simplified to remain a couple of planetary gears, in which TVMS and backlash of meshing gears are considered. It is shown by numerical predictions that with an increase of excitation frequencies, motions of the two planetary gears experience dynamic instabilities and bifurcations. Meanwhile, vibration amplitudes in velocities of the dynamic system increase doubly. Numerical

solutions are validated by experiments for accelerations and noise pressures acquired from the NVH bench test.

References

1. CUNLIFFE F., SMITH J.D., WELBOURN D.B., 1974, Dynamic tooth loads in epicyclic gears, *Journal of Engineering for Industry*, **96**, 2, 578-584

2. ERITENEL T., PARKER R. G., 2009, Modal properties of three-dimensional helical planetary gears, *Journal of Sound and Vibration*, **325**, 1-2, 397-420

3. FARSHIDIANFAR A., SAGHAFI A., 2014, Global bifurcation and chaos analysis in nonlinear vibration of spur gear systems, *Nonlinear Dynamics*, **75**, 4, 783-806

4. GU X., VELEX P., SAINSOT P., BRUY/'ERE J., 2015, Analytical investigations on the mesh stiffness function of solid spur and helical gears, *Journal of Mechanical Design*, **137**, 6, 063301

5. GUO H., ZHANG J., YU H., 2018, Dynamic modelling and parametric optimization of a full hybrid transmission, *Proceedings of the Institution of Mechanical Engineers, Part K: Journal of Multi-body Dynamics*, **233**, 1, 17-29

6. HEDLUND J., LEHTOVAARA A., 2008, A parameterized numerical model for the evaluation of gear mesh stiffness variation of a helical gear pair, *Proceedings of the Institution of Mechanical Engineers, Part C: Journal of Mechanical Engineering Science*, **222**, 7, 1321-1327

7. KAHRAMAN A., 2001, Free torsional vibration characteristics of compound planetary gear sets, *Mechanism and Machine Theory*, **36**, 8, 953-971

8. KASUBA R., EVANS J.W., 1981, An extended model for determining dynamic loads in spur gearing, *ASME Journal of Mechanical Design*, **103**, 2, 398-409

9. LIN J., PARKER R.G., 1999, Sensitivity of planetary gear natural frequencies and vibration modes to model parameters, *Journal of Sound and Vibration*, **228**, 1, 109-128

10. LIN J., PARKER R.G., 2000, Structured vibration characteristics of planetary gears with unequally spaced planets, *Journal of Sound and Vibration*, **233**, 5, 921-928

11. MEISEL J., 2011, Kinematic study of the GM front-wheel drive two-mode transmission and the Toyota hybrid system THS-II transmission, *SAE International Journal of Engines*, **4**, 1, 1020-1034

12. MUTA K., YAMAZAKI M., TOKIEDA J., 2004, Development of new-generation hybrid system THS II – drastic improvement of power performance and fuel economy, *SAE 2004 World Congress and Exhibition*, 2004-01-0064

13. ÖZGÜVEN H.N., HOUSER D.R., 1988, Mathematical models used in gear dynamics – a review, *Journal of Sound and Vibration*, **121**, 3, 383-411

14. WANG J., LI R., PENG X., 2003, Survey of nonlinear vibration of gear transmission systems, *Applied Mechanics Reviews*, **56**, 3, 309-329

15. WANG Q., ZHAO B., FU Y., KONG X., MA H., 2018, An improved time-varying mesh stiffness model for helical gear pairs considering axial mesh force component, *Mechanical Systems and Signal Processing*, **106**, 413-429

16. ZENG X., WANG J., 2018, *Analysis and Design of the Power-Split Device for Hybrid Systems*, Springer, Singapore

17. ZHANG J., GUO H., ZOU L., YU H., 2017a, Optimization of compound planetary gear train by improved mesh stiffness approach, *Proceeding of ASME International Mechanical Engineering Congress and Exposition, ASME*, Tampa, Florida, USA

18. ZHANG J., LIU D., YU H., 2017b, Experimental and numerical analysis for the transmission gear rattle in a power-split hybrid electric vehicle, *International Journal of Vehicle Design*, **7**, 1, 1-8

19. ZHAO F., HAO H., LIU Z., 2015, Technology strategy to meet China's 5 L/100 km fuel consumption target for passenger vehicles in 2020, *Clean Technologies and Environmental Policy*, **18**, 2, 7-15